Research article

polymers advanced technologies

Received: 22 February 2016, Revised: 25 March 2016, Accepted: 11 April 2016, Published online in Wiley Online Library

(wileyonlinelibrary.com) DOI: 10.1002/pat.3816

Electrospun poly(3-hexylthiophene)/poly (ethylene oxide)/graphene oxide composite nanofibers: effects of graphene oxide reduction

Filippo Pierini[a]*, Massimiliano Lanzi[b], Paweł Nakielski[a], Sylwia Pawłowska[a], Krzysztof Zembrzycki[a] and Tomasz Aleksander Kowalewski[a]

In this article, we report on the production by electrospinning of P3HT/PEO, P3HT/PEO/GO, and P3HT/PEO/rGO nanofibers in which the filler is homogeneously dispersed and parallel oriented along the fibers axis. The effect of nanofillers' presence inside nanofibers and GO reduction was studied, in order to reveal the influence of the new hierarchical structure on the electrical conductivity and mechanical properties. An in-depth characterization of the purity and regioregularity of the starting P3HT as well as the morphology and chemical structure of GO and rGO was carried out. The morphology of the electrospun nanofibers was examined by both scanning and transmission electron microscopy. The fibrous nanocomposites are also characterized by differential scanning calorimetry to investigate their chemical structure and polymer chains arrangements. Finally, the electrical conductivity of the electrospun fibers and the elastic modulus of the single fibers are evaluated using a four-point probe method and atomic force microscopy nanoindentation, respectively. The electrospun materials crystallinity as well as the elastic modulus increase with the addition of the nanofillers while the electrical conductivity is positively influenced by the GO reduction. Copyright © 2016 John Wiley & Sons, Ltd.

Keywords: electrospun composite nanofibers; poly(3-hexylthiophene); graphene oxide; electrical conductivity; mechanical properties

INTRODUCTION

Since the discovery that conjugated polymers can conduct electricity upon doping processes, these conductive macromolecules have been considered as innovative new materials that would lead to the next generation of electronic devices.[1] During the last decades, a large number of researchers have focused their studies on the field of intrinsically conducting polymers (ICPs). The recent development of organic electronic devices made by ICPs has contributed to the spread of conjugated polymer use from an academic curiosity to an effective application in the new electronics industry.[2]

Polythiophenes (PTs) are the most attractive ICPs in the field of organic electronic materials.[3] PTs hold outstanding thermal and environmental stability and electrical conductivity when doped, but their processability and properties are strongly affected by the structure and chemical modifications.[4] Consequently, materials with tailor-made properties can be designed by inserting substituents, such as alkyl groups, in the three position of a thiophene ring in order to obtain configurationally regular and soluble polymeric chains.[5] Poly(3-alkylthiophene)s (P3ATs) and, in particular, regioregular poly(3-hexylthiophene) (P3HT) have been used in a plethora of electronic and optoelectronic device applications. Undoubtedly, the possibility of preparing miniaturized devices plays a crucial role in the potential applications within these fields. P3ATs nanofibers have drawn great attention because of the prospects generated by the combination of organic conducting polymers and nanostructured materials that could yield functional materials with new unexpected properties.[6] The possibility to produce one-dimensional (1D) polymer nanomaterials not only opens the door to the fabrication of microscale and nanoscale devices but it also improves the properties of ICPs and increases the applicability of conjugated polymers in all the applications that involve polymer interactions with its environment.[7] The material 1D-nanostructuration leads to more efficient sensors[8] and solar cells[9] and is a fundamental prerequisite in the production of flexible and wearable devices.[10] In particular, the development of P3HT nanofibers has significant benefits in comparison with film-casting polymer, because the former technique leads to a highly active surface area.

* *Correspondence to: Filippo Pierini, Department of Mechanics and Physics of Fluids, Institute of Fundamental Technological Research, Polish Academy of Sciences, 02-106 Warsaw, ul. Pawinskiego 5B, Poland.*
E-mail: fpierini@ippt.pan.pl

a *F. Pierini, P. Nakielski, S. Pawłowska, K. Zembrzycki, T. A. Kowalewski*
Department of Mechanics and Physics of Fluids, Institute of Fundamental Technological Research, Polish Academy of Sciences, ul. Pawinskiego 5B, 02-106, Warsaw, Poland

b *M. Lanzi*
Department of Industrial Chemistry "Toso Montanari", Alma Mater Studiorum, University of Bologna, Viale Risorgimento 4, 40136, Bologna, Italy

Electrospinning is the most exciting nanofibers preparation technique. Electrospinning gained high interest during the last decade because it produces ultrathin fibers having a diameter a few orders of magnitude smaller than those obtained with conventional fibers fabrication techniques (from microns to less than 10 nm).[11,12] Furthermore, using this technique, it is possible to tune the materials' properties (e.g. the fibers alignment, porosity, and inner fibers structuration).[13] The strong stretching forces and the physical confinement into the cylindrical nanofibers generated by electrospinning strongly affect the orientation of polymer chains along the long axis of a fiber.[14] Mechanical, electrical, optical, and photoelectronic properties of ICPs are correlated to their molecular and supramolecular structure and crystallinity, therefore, processing PATs with electrospinning generates materials with improved or even with new features.[15] The improvement of the polymer chains orientation along the fiber is the best way to increase the electrical conductivity of P3HT because the charge mobility along the backbone is considerably higher than that along the $\pi-\pi$ stacking direction. Moreover, the strong stretch applied during the electrospinning process further improves the electrical properties owing to the simultaneous alignment and stretching of the polymer chains.[16]

Because P3HT has shown very high charge carrier mobility, it has been considered the strongest candidate for producing new organic electronic devices and solar cells. The morphology, chemical structure, electrical, thermal, mechanical, and physical properties of P3HT electrospun fibers have been studied to improve their applicability.[17] Several researches have put great efforts into the study of nanofibers made by P3HT blends in which the conjugated polymer is mixed with a material capable of increasing the electrospinnability of the solution. Polyethylene oxide (PEO) has been often chosen to produce uniform, defect-free, and reproducible nanofibers based on P3HT, because it can be easily removed by a post-electrospinning treatment.[18] This method usually involves selective washing with organic solvents that guarantees the complete removal of the insulating polymer and the production of thinner, pure P3HT nanofibers with improved electrical properties.

Moreover, electrospinning usually improves the mechanical properties of the fibers thanks to the crystallization and elongation processes involved in their production.[19] Experimental investigations have shown that the single electrospun fibers strength nonlinearly increases as the fiber diameter decreases.[20] Several studies have revealed an intimate relationship between the change of polymer crystallinity and the rise of the Young's modulus by decreasing the radius of the fibers. The increment of Young's modulus in ultrathin fibers is due to the strong orientations of both macromolecular chains and crystals. The formation of stiffer crystalline zones is also dependent on the polymer chemical properties, especially their molecular weight. Camposeo *et al.* have recently developed a model of the polymer elongation dynamics during electrospinning and have proved the presence of a core with close-packed molecules in electrospun conjugated polymer fibers.[21] This model does not only justify the increment of the stiffness in single ultrathin-fibers and the existence of unique electrical and optoelectrical properties of conductive electrospun fibers but also confirms the possibility to tune the electrical conductivity and mechanical properties by increasing molecular regularity and crystallinity.

The most common technique to improve the electrical and mechanical properties of electrospun conducting fibers is the incorporation of a second phase into the polymer matrix.[22] Fillers are usually made of a nanomaterial, which has higher electrical conductivity and stiffness than neat ICPs fibers. Carbon nanotubes are the most applied nanofillers in the field of electrospun ICPs-based composite fibers,[23] but their applicability is limited because of their poor processability.[24] Furthermore, the unique structure of ICPs allows the enhancement of the mechanical and electrical properties of the materials by simply increasing the crystallinity and stretching the polymer chains. Recently, the possibility to improve the electrical conductivity by including parallel aligned insulating nanotubes has been demonstrated, opening the way to the use of different and more easily processable materials as nanofillers.[25] Moreover, the progress made in the field of development of atomically thin layered carbon nanostructures such as graphene, graphene oxide (GO), and reduced graphene oxide (rGO) has drastically increased the applicability of conjugated polymer nanocomposites.

Graphene is the most fascinating material of the last decade, it attracts a great amount of researchers, and the number of publications, patents, and applications are exponentially increasing. Graphene is made of planar atomic thick single graphite layers of sp^2-bonded carbon atoms arranged in a honeycomb pattern. Graphene, due to its electrical (carrier mobility ~2.0×10^6 cm^2/Vs) and mechanical properties (Young's modulus of ~1.0 TPa), has been proposed as filler for different materials.[26] Unfortunately, the application of graphene for the production of 1D conductive polymer composites is influenced by the intrinsic tendency of the single nanosheets to be crumpled and folded and to form aggregates during the composite preparation, which negatively affects the performance of the final materials.[27] Moreover, the properties of graphene depend on the synthesis technique, which, in the case of high quality material, can be time-consuming and expensive, precluding its practical use.

Graphite oxide has a structure similar to that of graphene and the main difference is due to the presence of oxygen-containing functional groups, which allows this layered material to display new properties.[28] Unlike graphene synthesis, GO synthesis is easy and inexpensive; additionally, graphene oxide is easily dispersible in water and several organic solvents, as well as in polymer matrices, and the development of nanocomposites based on GO/polymer is reproducible.[29] The presence of a large functionalized area leads to consistent changes in the materials' properties, in fact, the mechanical properties of GO are poorer than those of graphene.[30] Most importantly, the presence of a high amount of functional groups entails a change in the electronic structure of graphene, and the electrical conductivity of GO, which exhibits typical dielectric properties (sheet resistance of ~1×10^{12} Ω sq^{-1}) due to the presence of sp^3 hybridized carbons platforms, drastically drops.[31] One of the most important features of GO is the possibility to be partially reduced to graphene-like sheets by removing the oxygen groups in order to recover the conjugated structure responsible for the electrical conductivity and other properties of graphene. The reduced GO (rGO) can have several levels of oxidation, and the reduction process can be carried out using a number of different strategies (e.g. thermal, chemical, photocatalyzed, electrochemical, and hydrothermal reduction).[32] Reducing GO to produce rGO is a fundamental process because it gives the possibility to tune the nanomaterials features to find the optimal balance between electrical, mechanical properties, and the formation of aggregates.[33]

Graphite oxide and rGO ICP composites are hot topics in polymer science. There is a great interest in developing P3HT-based

inorganic–organic nanocomposites, especially with GO and rGO, because filling a polymer matrix with layered nanomaterials greatly improves its mechanical and electrical properties and can also introduce new functionalities. For example, P3HT/GO[34] as well as P3HT/rGO[35] nanocomposites have been found to be useful for the development of organic field-effect transistors, supercapacitors, sensors, and photovoltaic devices. These composites showed considerable improvements in strength, electric conductivity, and thermal stability because of the wide interfacial surface between the fillers and the polymer chains. Moreover, in the case of nanofibers, the orientation of the GO and rGO along the fiber axis and its uniform distribution is sought to enhance the material features.

Herein, a simple method to include graphene oxide or reduced graphene oxide into electrospun P3HT/PEO nanofibers has been explored. In the first section, we reported a "green" technique to slightly reduce GO in order to avoid side effects due to the aggregation; this method can be the first step for the fabrication of ICP/rGO nanocomposites. Moreover, we present an electrospinning-based approach to form fibrous nanomaterials in which the fibers are homogenously filled with parallel oriented GO or rGO nanosheets. The proposed technique can be easily applied to other ICPs, and the produced fibers have great potential to be used as hybrid nanomaterials for miniaturized flexible organic electronic and photovoltaic devices.

The present study deals with the effect of the GO reduction on the final materials' properties, accounting its influence on the filler dispersion during the material preparation. It also aims to prove the relationship between the formation of an ideal architecture and the improvement of electrical conductibility and mechanical properties. Furthermore, we were able to confirm the fundamental role of the hierarchical structure generated by the parallel orientation of the nanofillers along the nanofibers and the correlated increment of the material crystallinity as well as the charge mobility along the fiber. Our results show that the crystallinity and the P3HT chains orientation as well as the mechanical properties of the nanofibers could be tuned by adding GO into the fibers; furthermore, the GO oxidation level can be modified in order to improve the electrospun fibers electrical properties.

EXPERIMENTAL

Materials

Regioregular P3HT was chemically synthesized, as described in the next section. All the solvents and reagents used for the polymer synthesis were purchased from Sigma-Aldrich (St. Louis, MO, USA). Tetrahydrofuran (THF) was distilled over Na/K alloy and stored over molecular sieves (4 Å) under nitrogen. PEO (Mw = 900 000 g/mol), iodine (I_2), and chloroform ($CHCl_3$) were purchased from Sigma-Aldrich. The single layer GO (99 wt. % purity) used in this study was purchased from Cheap Tubes Inc. (Cambridgeport, VT, USA), and its characteristics, provided by the supplier, were as follows: average nanosheets thickness: 1.1 ± 0.2 nm; elemental analysis: 35–42% carbon, 45–55% oxygen, and 3–5% hydrogen. The conductive silver paint was supplied by Ted Pella. All chemicals were used as received. Water was deionized using a Milli-Q Ultra-Pure-Water Purification 10 System (18.50 MΩ).

Monomer synthesis: 2,5-dibromo(3-hexyl)thiophene (2,5BT6H)

A solution of 1.12 g (6.4 mmol) of N-bromosuccinimide (NBS) in 8 ml of N,N-dimethylformamide (DMF) is added to a solution of 0.54 g (3.2 mmol) of 3-hexylthiophene (T6H) in 8 ml of DMF. After stirring for 30 h at room temperature and under a flow of dry nitrogen, the reaction mixture is poured into 120 ml of distilled water and extracted with 5 × 20 ml of $CHCl_3$. The organic phase is washed again with water (5 × 20 ml), dried with $MgSO_4$ and concentrated giving 1.02 g (2.8 mmol) of 2,5BT6H (88% yield).

^{1}H-NMR ($CDCl_3$, ppm): δ 6.80 (s, 1H, H4-Th); 2.48 (t, 2H, Th-CH_2); 1.75–1.25 (bm, 8H, central –CH_2-); 0.90 (t, 3H, $-CH_3$).

FT-IR (KBr, cm^{-1}): 3050 (ν_s C-H β-thiophene), 2933 (ν_{as} –CH_2-), 2857 (ν_s –CH_2-), 1545 (ν_{as} C = C thiophene), 1462 (ν_s C = C thiophene), 1433, 1420, 1375 ($-CH_3$ def), 1254, 1235, 1187, 1001 (aromatic ν C-Br), 829 (γ C-H thiophene), 723 ($-CH_2$- rocking).

Poly(3-hexylthiophene) synthesis

3.0 ml (3.0 mmol) of a 1M solution of methylmagnesiumbromide in di-n-butylether are added to a solution of 1.09 g (1.5 mmol) of 2,5BT6H in 20 ml of anhydrous THF. The reaction mixture is refluxed for 1 h with stirring and under a flow of nitrogen. 0.017 g (0.032 mmol) of [1,3-bis(diphenylphosphino)propane] nickel(II) chloride (Ni(dppp)Cl2) are then added and the mixture is refluxed again for 2 h. The reaction mixture, cooled down to room temperature, is poured into 150 ml of MeOH and filtered over a PTFE membrane (0.45 μm pore size). The recovered polymer was washed again with methanol and finally with n-hexane, giving 0.20 g (1.2 mmol) of P3HT.

^{1}H-NMR ($CDCl_3$, ppm): δ 7.05, 7.02, 7.00, 6.97 (4 s, 1H, H4-Th); 2.80, 2.55 (2bm, 2H, Th-CH_2); 1.70–1.20 (bm, 8H, central –CH_2-); 0.90 (t, 3H, $-CH_3$).

FT-IR (KBr, cm^{-1}): 3055 (ν_s C-H β-thiophene), 2925 (ν_{as} –CH_2-), 2854 (ν_s –CH_2-), 1512 (ν_{as} C = C thiophene), 1464 (ν_s C = C thiophene), 1431, 1422, 1377 (-CH_3 def), 1254, 1187, 827 (γ C-H thiophene), 723 (-CH_2- rocking).

Elemental analysis calculated for $(C_{10}H_{14}S)_n$: C, 72.23%; H, 8.49%; S, 19.28%. Found: C, 73.31%; H, 8.32%; S: 18.37%.

Graphene oxide hydrothermal reduction

25 mg of as-received GO was suspended in 25 ml of water. The GO suspension was sonicated for 30 min using an ultrasonic probe processor (Dr. Hielscher processor model UP 200H), and then the brown colloidal solution was sealed in a Teflon lined autoclave (Parr reactor model 4652). The GO reduction was performed at 160 °C for 6 h. After the hydrothermal reduction, the obtained dark sol was treated with the ultrasonic probe for 5 min and then centrifuged at 2000 rpm for 5 min in order to remove any undispersed materials. Finally, the rGO was washed with water several times, and the obtained sample was dried at 40 °C for 24 h. The procedure was repeated performing the reduction at different temperatures (140 °C and 180 °C), but the rGO samples obtained in these syntheses were not used as polymer matrix fillers because they did not show a relevant grade of reduction and tend to form undesirable crumpled, folded, and aggregated structures, respectively.

Preparation of electrospun nanofibers

The first step was the preparation of the solution used to produce the P3HT/PEO nanofibers: 200 mg of poly(3-hexylthiophene) were dissolved in 10 ml of chloroform, and the solution was stirred for 24 h at 50 °C. After that, 200 mg of poly (ethylene oxide) were added, and the solution was stirred for further 24 h.

The composite solutions were prepared by adding 3.0 mg of nanofiller (GO or rGO) to 2 ml of chloroform into a vial followed by sonication. To reach a stable and homogenous dispersion of rGO, it was necessary to treat the colloidal system with the ultrasonic probe for 30 min while the GO sol was processed for 60 min. Then 20 mg of P3HT were added to the suspension and stirred at 50 °C for 24 h. In the subsequent step, 20 mg of PEO were introduced into the flask, and the whole solution was stirred again for 24 h. The concentration of GO/rGO in the polymer solutions was previously optimized in order to develop the desired 1D-nanstructured composites. Nanofibers produced with lower amounts of nanofillers were not completely filled with the layered nanomaterials, although the use of higher concentrations of GO (or rGO) led to the formation of morphological imperfections in the fibers due to the polymer matrix overloading.

All the solutions were immediately electrospun in order to avoid the formation of aggregates. The polymer-based solutions were introduced into a syringe connected with a needle. The syringe was accommodated in an automatic pump (KD Scientific syringe pump model 200-CE), and the needle was connected to a high voltage power supply (Spellman model SL150) in order to perform the electrospinning procedure. The fibers were deposited on a grounded metal collector screen. For the nanomechanical tests, carried out by atomic force microscopy nanoindentation, a small number of fibers were collected on a 1 cm^2 glass slide, placing the substrate onto the metal plate.

The electrospinning processes were performed applying different experimental parameters (needle to target distance, D; polymer solution flow rate, Q; and applied voltage, E) during the production of P3HT/PEO (D = 18 cm; Q = 0.5 ml/h; and E = 19.5 kV), P3HT/PEO/GO (D = 18 cm; Q = 0.5 ml/h; and E = 17 kV), and P3HT/PEO/rGO (D = 16 cm; Q = 0.5 ml/h; and E = 19 kV) nanofibers.

Morphological characterizations

The GO and rGO nanosheets morphology, dimensions, aggregation tendency, and the presence of nanofillers inside the electrospun fibers were evaluated by observing the samples deposited on carbon coated copper grids using a Philips CM100 transmission electron microscope (TEM; Philips Electron Optics, Eindhoven, The Netherlands) operating at an accelerating voltage of 100 kV for the inorganic materials and 80 kV for the composites. The samples were analyzed at different magnifications. A scanning electron microscope (SEM; Carl Zeiss SMT Ltd., Cambridge, UK) was used to assess the surface morphology of the electrospun mats as well as to measure the fibers diameter. The samples were sputter coated with a 5 nm thick gold layer before the SEM analyses in order to avoid the materials charging and to increase the micrographs quality. To assess a statistically reliable value of the average fibers diameter, at least 200 individual fibers were measured.

Spectroscopic characterizations

^{1}H-NMR spectra were recorded at room temperature, in 5–10% $CDCl_3$ solutions, by means of a Varian Mercury 400 (400 MHz) spectrometer; chemical shifts are reported in ppm units with TMS as the internal standard.

The Fourier transform infrared (FT-IR) spectra of 2,5BT6H and P3HT were recorded on KBr disks by a Perkin Elmer Spectrum One spectrophotometer. Average molecular weights and polydispersity of the P3HT were determined by gel permeation chromatography (GPC) analysis using THF solutions on a UV–Vis Linear Instrument UVIS-200 operating at 254 nm, equipped with a Phenomenex Phenogel Mixed bed column, 5 μ MXL type. The calibration curve was recorded using monodisperse polystyrene standards. The X-ray diffraction (XRD) patterns of the polymer materials were carried out by a PW1050/81-PW1710 diffractometer (Philips, Eindhoven, The Netherlands), using Cu Kα radiation.

The GO and rGO chemical structures were studied recording Raman spectra from 1200 to 1650 cm^{-1} on a NT-MDT Ntegra system at room temperature.

Fourier transform infrared of GO and rGO were recorded on a Thermo Scientific Nicolet 380 FT-IR Spectrometer by using pressed pellets prepared by mixing 1.0 mg of sample with 150 mg of infrared grade KBr in order to determine the chemical functionalization of the graphene-like nanosheets.

Thermal analyses

In order to assess the thermal stability, purity and amount of oxygen-containing functional groups of GO and rGO, thermogravimetric analyses (TGA) were carried out. The TGA analyses were performed using a TA Instruments SDT Q600. Around 5.0 mg of samples were placed in an Al_2O_3 pan and heated from 20 °C to 800 °C at a rate of 10 °C/min under a nitrogen flow (100 ml/min).

Polymer materials differential scanning calorimetry (DSC) was conducted on a DSC TA Instruments Q 2000 in the $-50 \div 300$ °C range at a heating/cooling rate of 10 °C/min under nitrogen atmosphere. The analyses were performed in sealed aluminum pans with a sample weight varying in the $2 \div 5$ mg range.

Nanomechanical tests

Atomic force microscopy nanoindentation analyses were carried out using a NT-MDT Ntegra AFM, in order to evaluate the elastic modulus (E) of the single electrospun nanofibers collected onto the glass slides. Firstly, topographical reconstructions of the samples were performed to select the indentation zones by means of an AFM equipped with a silicon tip (NT-MDT model NSG01) operating in tapping mode. Subsequently, the same AFM instrument setup, operating in contact mode, was used to indent the fibers and record the typical force–distance curves. The elastic moduli were calculated examining the slope of the loading curves and fitting these data into the Hertz model.[36] The results were obtained averaging more than 50 indentations curves per sample acquired analyzing several fibers.

The cantilevers were previously calibrated using a thermal method in order to calculate their spring constant (k, varying from 0.8 N/m to 3.0 N/m) and their sensitivity was evaluated by indenting a glass substrate. Moreover, the cantilevers were characterized before and after the indentations by SEM and scanning a test silicon grating (NT-MDT, TGT1) to evaluate their dimensions and to ensure that their structural and morphological properties were unchanged during the indentations.

Measurements were performed 24 h after the electrospinning procedure in air at 25 °C.

Electrical conductivity testing

The electrical properties of the electrospun samples were evaluated on the mats by a standard four-point method. Data were acquired using a Keithley 2401 sourcemeter connected to an Alessi Instruments C4S four-point probe head (probe material: osmium; probe tip spacing: 1.6 mm; spring pressure: 40–70 g; probe tip diameter: 0.2 mm).[37] The samples were produced by collecting at least 50 mg of polymer blend/composite nanofibers onto glass slides. The fibers depositions were performed by placing the insulating substrates on the surface of the metal collector during the electrospinning process. The cross-sectional thickness of the analysed mats was quantified via SEM microscopy. The micrographs of the mats demonstrated homogeneous fiber distribution inside the materials and that the mats thickness ranges from 100 μm to 150 μm. Furthermore, the contact between osmium points and the mats surface were improved by using a silver paint micro deposition technique in order to cover the probe surface with a small amount of conductive paint and minimize problems associated with the probe-sample connection. The final results were calculated averaging the data obtained measuring the conductivity in at least 10 different locations on three different mats per each sample. The measurements of the materials were performed 24 h after the production of the mats by electrospinning. The doped electrospun materials were tested approximatively two minutes after the doping treatments. Electrical conductivity measurements were carried out under ambient conditions. The doping treatments were performed by leaving iodine crystals and the produced electrospun mats in a close chamber at 40 °C for 5 h. Previous experiments revealed that the exposition to the I_2 vapors of the samples in these conditions was enough to reach the maximum doping level.

RESULTS AND DISCUSSION

Features of the starting polymers and nanofillers

The polymer P3HT was synthesized by refluxing the 2,5BT6H monomer with one equivalent of methylmagnesium bromide in anhydrous THF.[38] The obtained reactive monomer is the organometallic intermediate giving the final polymer upon addition of a catalytic amount of Ni(dppp)Cl_2. FT-IR and ^{1}H-NMR analysis of 2,5BT6H and P3HT are reported in the Experimental section as well as the elemental analysis of the polymer. The performed analysis agrees with the expected chemical structures. Moreover, the degree of regioregularity of P3HT (96%HT) was evaluated on the basis of the intensity ratio of the two signals in the 2.80–2.55 ppm range ascribable to the methylenic protons in α to the thiophene ring. In fact, the signal in the lower fields is assigned to the HT dyads, while the other to HH and TT dyads. Molecular weight characteristics of the polymer were obtained by GPC and the obtained values (M_n = 32000 g/mol, PDI = 1.2) are in good agreement with those usually obtained with this polymerization procedure.[39]

Colloidal suspensions of GO and rGO prepared using ultrasound treatment were used as the starting material for the composites. We used TEM to evaluate the morphology, dimension, exfoliation and tendency to aggregation of the nanosheets. Figure 1 shows the typical TEM micrographs of GO (Fig. 1A) and rGO (Fig. 1B). Both the TEM images display well-dispersed nanolayered materials. The GO and rGO are composed by square or rectangular shape nanosheets having a surface area of around 1.0 μm^2. The materials are dimensionally homogeneous and the sheets maintained their typical unfolded and uncrumpled shape even in the reduced state; moreover, aggregates were not present in the analysed sols. The TEM micrographics clearly show that the sheets morphology was still preserved after the hydrothermal treatment, and this allowed us to consider GO and rGO morphologically equivalent.

Fourier transform infrared spectroscopy, Raman spectroscopy, and TGA were performed in order to reveal the reduction of GO after the hydrothermal treatment as well as assessing the chemical structure, thermal stability and the purity of the nanofillers.

Figure 2 shows the typical FT-IR spectra of GO (red line) and rGO (black line).[40] Both the acquired spectra are characterized by the presence of absorption peaks at similar wavelengths that confirm the presence of oxygen-containing groups on the nanosheets surface. The most oxygen-containing groups absorption peaks can be found at ~3400 cm^{-1} (O-H stretching vibrations, broad peak), ~1350 cm^{-1} (O-H bending vibrations), ~1730 cm^{-1} (C = O stretching vibrations of carbonyl and carboxylic groups), ~1220 cm^{-1} (C-O stretching vibrations), and ~1000 cm^{-1} (C-O stretching vibrations). The intensities of the peaks attributable to hydroxyl, carboxyl, carbonyl, and ether function groups decreased strongly after the reduction. FT-IR spectroscopy indicates the presence of different types of oxygen functionalities on the GO material and suggests that oxygen-containing groups are less abundant in rGO. This is confirmed by the increase of the relative intensity of the skeletal vibrations peaks due to the unoxidized graphitic domains (C = C stretching vibration at ~1630 cm^{-1}). Moreover, the intensity of the peak at

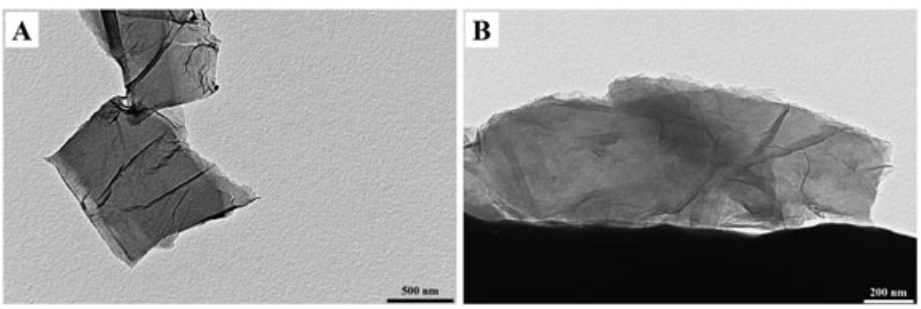

Figure 1. Transmission electron microscope images at different magnification of graphene oxide (A – scale bar: 500 nm) and reduced graphene oxide (B – scale bar: 200 nm) before and after hydrothermal treatment, respectively.

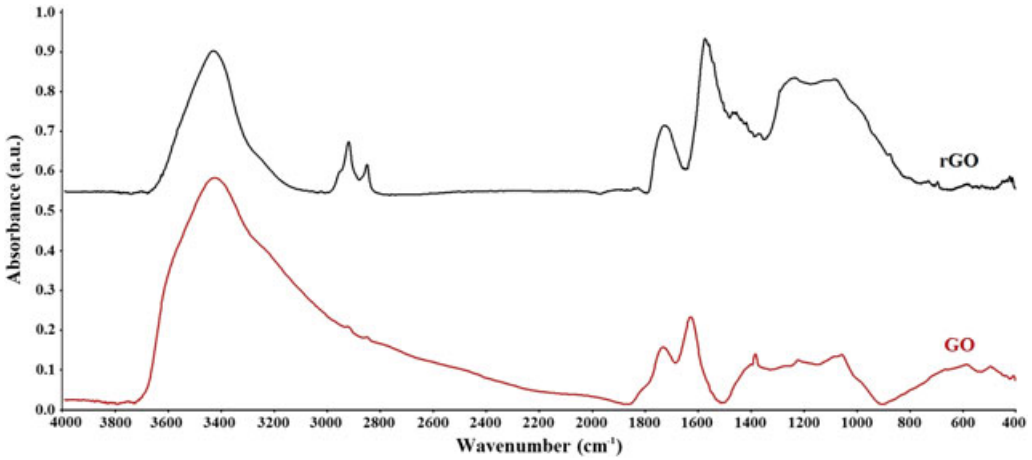

Figure 2. Fourier transform infrared spectra of graphene oxide (GO; red line) and reduced graphene oxide (rGO; dark line) treated hydrothermally. This figure is available in colour online at wileyonlinelibrary.com/journal/pat

~1630 cm^{-1} present in the GO spectrum could have been influenced by the deformation vibration (ν_2) of absorbed water.

Similarly to FT-IR, Raman spectroscopy provided evidence of the real reduction occurred during the thermal treatment; moreover, it gave us information about the graphitic skeletal structure of the nanosheets. Both the Raman spectra of GO and rGO (Fig. 3) exhibit a D band at ~1320 cm^{-1} and a G peak at ~1580 cm^{-1}. The D band corresponds to the breathing mode of κ-point phonons of A_{1g} symmetry and indicates the presence of disorder in the graphene sheets generated by defects such as vacancies and amorphous carbon species. The broad G band is ascribable to the first-order scattering of the E_{2g} mode of carbon atoms.[40] The change of the relative intensities of D and G peaks (I_D/I_G) in the Raman spectra is a reliable indicator of the reduction level of graphene and its derivatives; in fact, it can be associated to the degree of disorder as well as to the presence of sp^2 carbon domains into the carbon network.[41] Figure 3 shows a higher value of I_D/I_G in the rGO ($I_D/I_G = 1.15$) spectrum than in the GO curve ($I_D/I_G = 1.07$), this result is related to the increment of sp^2 domains determined by the reduction of the material after the hydrothermal treatment, which had effectively removed the oxygen groups from the nanosheets.

Finally, GO and rGO were analyzed by thermogravimetric analysis in order to verify their thermal stability, confirm the material reduction during the hydrothermal treatment and quantify the efficiency of this reaction. The first mass loss at around 100 °C is visible in both the produced TGA curves (Fig. 4). This change is attributed to the removal of water molecules absorbed inside the GO structure. The second mass loss, visible in both GO and rGO analysis, occurs at around 200 °C and is ascribable to the decomposition of the labile oxygen-containing groups in the forms of CO and CO_2.[42] GO loses 30% of its total weight between 125 °C and 240 °C, while rGO loses less than 15% of its mass in this region. TGA results do not only prove the good thermal stability of these materials, especially rGO, but also the efficiency of the applied reduction method,[41] indeed GO contains twice as much the amount in weight of oxygenated carbon species than rGO.

Electrospun nanofibers properties

The developed electrospun materials were firstly characterized by use of scanning and transmission microscopes. The morphological features of electrospun fibers are strictly dependent on several experimental parameters such as polymer solution

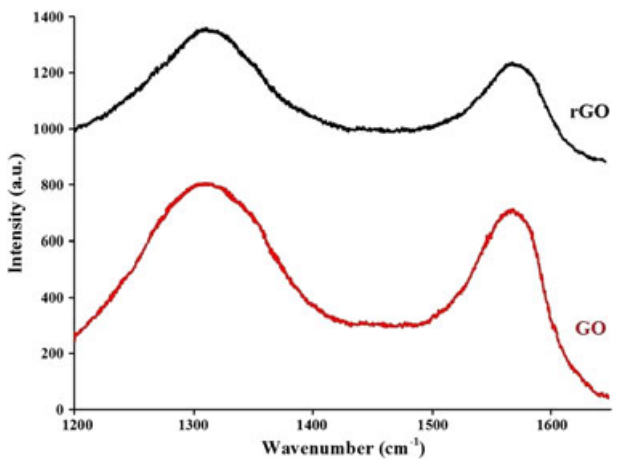

Figure 3. Raman spectra of graphene oxide (GO; red line) and reduced graphene oxide (rGO; dark line). This figure is available in colour online at wileyonlinelibrary.com/journal/pat

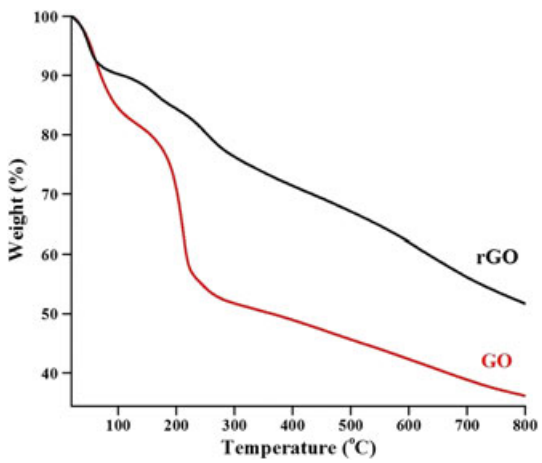

Figure 4. Thermogravimetric curves of graphene oxide (GO; red line) and reduced graphene oxide (rGO; dark line). This figure is available in colour online at wileyonlinelibrary.com/journal/pat

viscosity, needle to target distance, polymer solution flow rate, and applied voltage. In order to obtain nanofibers without beads or other defects, the procedure was optimized before the production of the samples. We have found that process reproducibility is not strongly influenced by slight variations of environmental conditions (e.g. temperature and humidity) and applied voltage in the range of 15–25 kV. The collected SEM pictures were used to assess the surface properties of the fibers, their alignment into the mat, and to quantify their diameter.

As it is shown in Fig. 5, the P3HT/PEO fibers are randomly deposited on the collector producing a uniform mat. The neat polymer nanofibers with average diameters of 688 ± 95 nm are straight and show a constant cylindrical morphology. The presence of PEO is vital for the production of nanofibers with the used setup because of the increase of the polymer solution spinability.[18] Despite the fact that the typical ICP/PEO phase separation in ultra-thin fibers is not appreciable with this technique, the contribution of the blend physical properties to the fibers morphology is visible, as the surface of the fibers displays a slight roughness, similar to that reported in other studies.[43]

Scanning electron microscope images of composite nanofibers made by GO and rGO were used to evaluate the morphology of the produced 1D nanostructured materials. Because the main objective of the composites preparation was to produce fibers completely filled with well-dispersed and parallel-aligned nanosheets, we have produced starting solutions with a high filler-to-polymer ratio. During the optimization of the electrospinning process, we faced the problem related to the presence of a high amount of nanofillers. The main structural defects related to the presence of GO or rGO (e.g. filler agglomerations and fibers breakage) were avoided by decreasing the concentration of P3HT and PEO, in comparison with the neat P3HT/PEO solutions, but maintaining the same P3HT : PEO ratio. This procedure, together with the good level of fillers dispersibility in the media, avoids the increase of the solution viscosity as well as its inhomogeneity that cause the drastic decline of the jet quality. Figures 6a and b show SEM images of the electrospun fibers produced with P3HT/PEO/GO and P3HT/PEO/rGO, respectively. As it is shown in the micrographies, the fibers have no defects such as beads and nanomaterials aggregates. Both the mats display a similar morphology, which confirms that it is possible to produce GO-based composite nanofibers with different reduction level without compromising their hierarchical structures. Nanofibers have a cylinder-like morphology, but their surfaces display increased roughness and shape irregularities when compared with the neat fibers. Different studies demonstrate that the decrease of the electrospun fibers diameter when adding nanofillers leads to an increased electrical conductivity of the material, due to the more effective stretching forces between the needle and the collector. Instead, the average diameters of the GO- and rGO-based composite nanofibers are larger (P3HT/PEO/GO: 1087 ± 245 nm and P3HT/PEO/rGO: 1112 ± 301 nm) than the mean diameter of the P3HT/PEO nanofibers. Comparing Fig. 6a and b, it is evident that the nanofibers created using GO and rGO have comparable morphological features, but both appear less straight than the unfilled fibers.

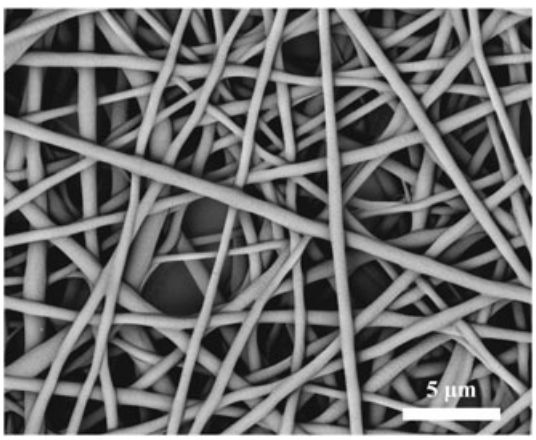

Figure 5. Scanning electron microscope micrograph of electrospun P3HT/PEO fibers (scale bar: 5.0 μm).

The morphological structure of ICPs fibers and the nanofillers geometrical disposition play a fundamental role in relation to the physical properties of the material such as their electrical conductivity and their stiffness. TEM analyses were performed in order to confirm the presence of the nanosheets into the fibers. As shown in Fig. 6c and d that refers to P3HT/PEO/GO and P3HT/PEO/rGO nanocomposites, respectively, both types of fibers are filled with layered nanomaterials. TEM images confirm the results obtained with SEM analysis proving the existence of a similar inner structure between the fibers obtained with GO and rGO. TEM images of the composites showed that the fillers are dispersed in the nanofibers without agglomeration; moreover, the presence of the GO or rGO is uniform and continuous into the fibers while gaps of unfilled polymer matrix are not visible. During the process optimization, we noticed that the presence of aggregates can be avoided by decreasing the polymer viscosity, increasing the efficiency of the colloids ultrasound treatment and using freshly prepared starting solutions. Our recent study similarly demonstrated that inorganic nanotubes were parallel oriented along the fiber axis of the ICP/PEO electrospun nanofibers by the effect of the external electric field and the resulting shear force.[25] TEM analyses were very useful to figure out the reason of the fiber diameter increase and the presence of the surface irregularities in the composite fibers. TEM images demonstrate the presence of GO and rGO nanosheets into the fiber and that their size is bigger than the neat fibers diameter. To begin with, the nanosheets are physically larger than the typical cylindrical fibers, and they are protruding out of the fibers. The high amount of fillers causes the typical irregular shape of these fibers in which several GO or rGO sheets stick out from the polymer matrix. However, the fact that there are GO nanosheets with high reduction level into the polymer structures of P3HT/PEO/GO and P3HT/PEO/rGO does not affect the smoothness and the dimension of the composite nanofibers as well as their distribution in the mats.

In order to investigate the inner structure of the prepared nanofibers, we analysed the produced fibrous mats and the pristine polymer powders by XRD. As it can be seen in Fig. 7, several diffraction peaks are observable for pure P3HT at $2\theta = 5.32°$ (100), 11.30° (200), 16.50° (300), and 23.41° (010). The (100) reflection of P3HT is due to the parallel polymer chains orientation. In particular, this signal corresponds to self-organized lamellar structures generated by the parallel stack of P3HT chains separated by hexyl side chains. Another important signal is the (010) peak that is due to the interchain $\pi-\pi$ stacking of P3HT, which indicates the distance between the faces of the thiophene rings. This signal, as well as the (100) peak, is an indicator of the crystalline structure presence in P3HT. The (200) peak can be associated to the distance between the lateral hexyl chains.

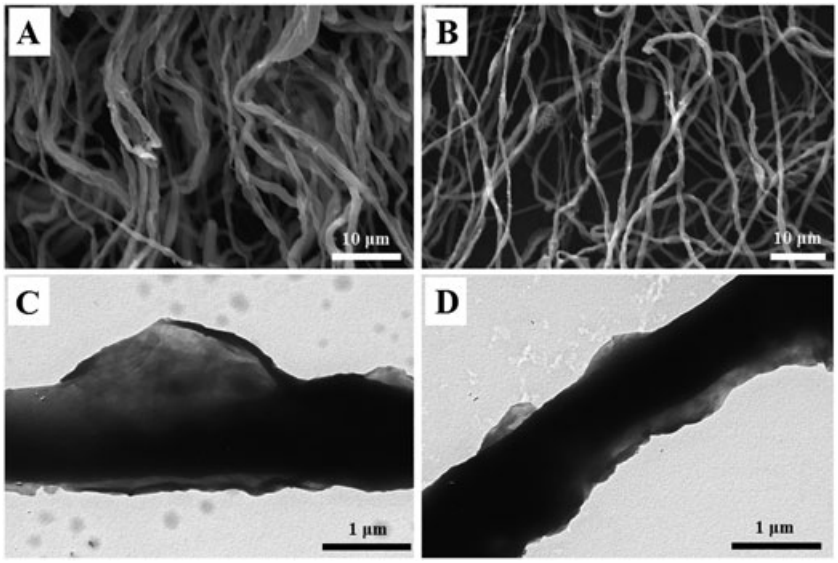

Figure 6. Scanning electron microscope images of P3HT/PEO/GO (A), P3HT/PEO/rGO (B) and TEM images of P3HT/PEO/GO (C), P3HT/PEO/rGO (D).

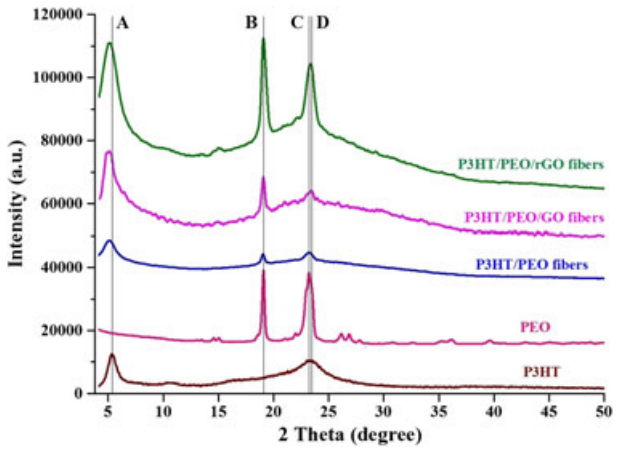

Figure 7. X-ray diffraction patterns of pristine P3HT (brown line), PEO (pink line), and electrospun P3HT/PEO (blue line), P3HT/PEO/GO (violet line) and P3HT/PEO/rGO (green line) mats. Two vertical straight lines are centered on the main peaks of pure P3HT (A and D), while the lines B and C are centered on the two main peaks of PEO. This figure is available in colour online at wileyonlinelibrary.com/journal/pat

As shown in Fig. 7, the typical semicrystalline diffraction peaks of pure PEO are observed at $2\theta = 19.10°$ and 23.21°. Furthermore, three weak peaks are visible in the $2\theta = 25–29°$ range. The XRD diffraction pattern of the electrospun P3HT/PEO nanofibers is displayed in the same figure. The electrospun mat diffractogram shows the presence of both P3TH and PEO; actually, all the main peaks of the two compounds are present. The (010) peak of the conductive polymer and the second main signal of PEO are overlapped. The pattern shows an amorphous halo centered at around $2\theta = 22°$: this signal suggests that the rapid evaporation of the solvent, which occurs during the electrospinning procedure prevents the formation of long-range order polymer chains packing. Despite this, the (100) diffraction peak due to the poly(3-hexylthiophene) lamellar orientation is visible. Furthermore, the shifts of the (100) maximum intensity peak at lower 2θ between the electrospun blend, and the pure P3HT prove the presence of elongated PEO chains between the P3HT structures.

The XRD spectra of GO and the rGO electrospun composites are shown in Fig. 7. The characteristic peak (002) of GO at around $2\theta = 11°$ and the typical (002) plane peak for rGO at around $2\theta = 24°$ do not appear in the XRD spectra of the composites, while all the peaks related to the polymers are visible. The absence of the fillers-related signals indicates that GO and rGO are not aggregated and they are excellently exfoliated.[35] Furthermore, the lack of these signals suggests the formation of an intercalated polymers-fillers structure into the electrospun fibers.[44] The assessment of this structure is highlighted by the small shift at lower 2θ of the (100) signal of P3HT in the composites when compared with that of the neat fibers. This shift is generated by the presence of exfoliated sheets of GO (or rGO) between the P3HT structures, although the small value of this shift is due to the irrelevant number of filler nanolayers in comparison with the consistent amount of P3HT chains in the composite matrix. The addition of nanofillers to the polymer blends before electrospinning leads to the increment of the polymers crystallinity. The improvement of the polymer chains arrangements is proved by the main diffraction signals changes that results in sharper peaks, while the polymers signals are more protruding if compared with the amorphous halo in the XRD patterns of P3HT/PEO/GO and P3HT/PEO/rGO.

The improved crystallinity obtained by the addition of GO and rGO into the fibers' structure was further verified by thermal analysis. The thermal properties of the produced nanomaterials were studied by differential scanning calorimetry. Figure 8 shows the DSC thermograms of P3HT/PEO, P3HT/PEO/GO, and P3HT/PEO/rGO electrospun fibers. DSC analyses were conducted not only to evaluate the thermal stability of the materials but also to investigate their crystallinity, studying the thermal transitions from a quantitative point of view. Table 1 reports the main transition temperatures and the related enthalpies of fusion (ΔH_m) of the developed fibrous materials. The DSC curve of the P3HT/PEO mat exhibits two endothermic transitions centered at 63.99 and 231.16 °C due to the melting of PEO (T_{m1}) and P3HT(T_{m2}), respectively.[45,46]

The thermograms of the two produced nanocomposites prove that higher thermal stabilities were achieved by including GO and rGO nanosheets into the polymer matrix, as the first

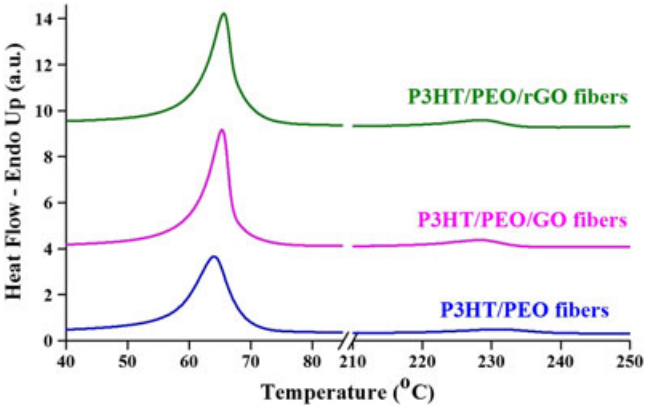

Figure 8. Differential scanning calorimetry curves of the electrospun P3HT/PEO (blue line), P3HT/PEO/GO (violet line), and P3HT/PEO/rGO (green line) mats in the T_{m1} and T_{m2} regions. This figure is available in colour online at wileyonlinelibrary.com/journal/pat

Table 1. Electrospun materials thermal properties obtained by differential scanning calorimetry. Main thermal transitions (melting points, T_m; enthalpies of fusion, ΔH_m) are indicated

Sample	T_{m1} (°C)	ΔH_{m1} (J/g)	T_{m2} (°C)	ΔH_{m2} (J/g)
P3HT/PEO	63.99	60.90	231.16	4.57
P3HT/PEO/GO	65.55	77.19	228.58	7.28
P3HT/PEO/rGO	65.22	77.94	228.26	7.93

transitions are shifted at higher temperature values. Most importantly, the values of the enthalpy related to both signals increase when nanofillers are present into the fibers. The higher ΔH_m prove the achievement of a higher degree of polymer crystallization into the composites in comparison with the unfilled fibers, thus confirming the previous results obtained by XRD.

The increase in crystallinity may be attributed to the well-known nucleation effect on the crystallization due to the presence of a nanostructured inorganic phase within the polymer matrix.[47] Moreover, nanosheets can act as a barrier to the solvent evaporation during the electrospinning process. The slowdown of the evaporation as well as the possible presence of solvent traces within the fibers core after the electrospinning process promotes the development of fibers with a higher degree of crystallinity.

The nanomechanical properties of single fibers were studied in order to figure out the contribution of the nanofillers to the physical features of the materials (Table 2). The elastic modulus value obtained for P3HT/PEO electrospun fibers is 0.68 ± 0.14 GPa. In spite of the fact that the mechanical properties of these fibers have not yet been studied (to the best of our knowledge) and that the stiffness of the electrospun fibers is strongly influenced by a number of factors (e.g. polymer crystallinity and fiber diameter), the elastic modulus values resulting from our calculations are as we expected.[48]

Table 2 clearly shows that when adding both types of nanofillers, the stiffness of the electrospun fibers increases resulting in a marked improvement in the materials' properties. The elastic modulus of P3HT/PEO/GO is more than double that of neat fibers, and the P3HT/PEO/rGO have similar stiffness. The AFM nanoindentation reveals that the electrospun materials' mechanical properties are strongly affected by the inclusion of GO or rGO into the fibers. This increment is consistent with similar materials' results reported in literature.[44] It is not surprising that the stiffness of the composite fibers is more marked, as XRD and DSC have proved the establishment of more crystalline structures that contribute to the stiffening of the materials. Moreover, the Young's modulus of GO and rGO single nanosheets is at least twice as high as the studied polymer blend, therefore, the reinforcing contribution of these layered materials is consistent. If the mean values of the elastic modulus are particularly relevant in order to assess mechanical properties, the obtained standard deviations give us important information about the composites structure. AFM nanoindentation is an extremely sensitive technique capable of providing information on a specific local point of the materials. As it is visible in Table 2, standard deviations (σ) of the composites measurements are similar to those of unfilled fibers (the σ of the three samples result are around 15–20% of their respective mean values) confirming the uniformity of the composites and the absence of aggregates. Furthermore, the values of the single measurements made on the composites never overlap the neat fibers results, confirming that the composites fibers are completely filled by the nanosheets and there are no unfilled gaps in these fibers. It is in fact well-known that the higher the GO reduction degree, the greater its stiffness,[30] but in our case there is no statically appreciable difference between P3HT/PEO/GO and P3HT/PEO/rGO stiffness values. This fact can be explained considering that the reinforcing contribution given by the fillers is smaller than the impact of the improved crystallinity on the fiber stiffness, thus confirming the fundamental role of the polymer matrix structure; moreover, because of the relative low quantity of the fillers as well as the non-complete reduction of the rGO, we cannot detect a consistent change of the elastic modulus comparing P3HT/PEO/rGO with P3HT/PEO/GO.

Finally, the electrical properties of the electrospun mats were studied by four-point method. It is important to remember that this characterization is helpful to measure the electrical conductivity of the whole analyzed mat surface, therefore the final value can be influenced by the microscopic and macroscopic structures of the samples (e.g. fibers disposition into the mat). It is

Table 2. Mechanical (elastic modulus) and electrical (conductivity) properties of the electrospun nanomaterials. Data are reported as mean ± standard deviation

Sample	Elastic modulus (GPa)	Electrical conductivity before doping (S/cm)	Electrical conductivity after doping (S/cm)
P3HT/PEO	0.68 ± 0.14	$1.85 \times 10^{-9} \pm 1.6 \times 10^{-10}$	$1.84 \times 10^{-2} \pm 1.2 \times 10^{-3}$
P3HT/PEO/GO	1.45 ± 0.22	$1.13 \times 10^{-9} \pm 1.7 \times 10^{-10}$	$6.08 \times 10^{-3} \pm 9.7 \times 10^{-4}$
P3HT/PEO/rGO	1.53 ± 0.26	$3.21 \times 10^{-7} \pm 5.8 \times 10^{-8}$	1.29 ± 0.19

for this reason, as well as for the intrinsic porous nature of the electrospun mats, that the measured electrical conductivities of the mats are lower than the corresponding single fibers conductivity. The measured electrical conductivity results of as-spun nanofibrous mats and of the same sample after iodine vapors doping are shown in Table 2. The conductivity of undoped P3HT/PEO mats is $1.85 \times 10^{-9} \pm 1.6 \times 10^{-10}$ S/cm, while the conductivity was found to increase by seven orders of magnitude after doping, reaching the value of $1.84 \times 10^{-2} \pm 1.2 \times 10^{-3}$ S/cm. These values fit very well with the results obtained by Laforgue *et al*., who has provided an extensive evaluation of the effect of P3HT : PEO ratio in these conductive fibers.[43] GO filled fibrous materials show a slight decrement of electrical conductivity that was calculated to be $1.13 \times 10^{-9} \pm 1.7 \times 10^{-10}$ S/cm for the undoped mats and $6.08 \times 10^{-3} \pm 9.7 \times 10^{-4}$ S/cm for the doped material. Since it is already proved that the incorporation of GO into the ICPs matrices does not provide benefits in terms of conductivity, the electrical properties of P3HT/PEO/GO are in the same order of magnitude as the neat mats conductivity. The incorporation of dielectric nanomaterials in the ICPs matrix usually determines a drastic drop in conductivity, because the nanofillers act as barriers limiting the charge hopping transport into the material, leading to an ineffective process. As we have previously demonstrated,[25] the spatial disposition of 1D-nanostructured or 2D-nanostructured fillers along electrospun ICP fibers can compensate the effect of the dielectric nanofillers owing to the formation of an ordered hierarchical structure inside the fibers. When GO nanosheets are oriented along the fiber axis, the polymer chains are more densely packed within the fibers through the GO layers confinement effect, and the crystallinity is higher too. In this structural situation, the negative barrier effect of the dielectric fillers is mitigated by the formation of compact and crystalline zones where the interactions between the P3HT chains are closer and the charge hopping is more effective.

The calculated electrical conductivity of P3HT/PEO/rGO is two orders of magnitude higher than the previously reported undoped nanofibrous mats, with a value of $3.2 \times 10^{-7} \pm 5.8 \times 10^{-8}$ S/cm. The highest electrical conductivity value of our experiment was recorded for this sample after doping it with I_2 (electrical conductivity: 1.29 ± 0.19 S/cm). The considerable improvement in the electrical properties is due to the synergic effect of the enhanced polymer crystallinity, parallel orientation of the nanosheets, and the intrinsic electrical conductivity of the nanofillers. In this case, the rGO sheets do not behave as physical obstacles for the movement of the charges, but they consistently help this process generating preferential pathways for the charge hopping along the direction of the electrical current flow (e.g. the fiber axis) that is confined between conductive walls (rGO), which can accelerate this process due to the recovered graphene-like conjugated structure.

As shown in Table 2, the electrical conductivity standard deviations of the composite samples result are around 15% of their respective mean values, while this value is around 10% for the neat fiber mats. As we have already stated, 4-probe methods results are affected by mats morphology. The similar standard deviations prove that, in spite of the well-known difficulties in producing stable electrospun composites, the produced GO-based and rGO-based mats do not show inhomogeneity resulting from side effects such as filler aggregations and fibers breakage.

It is worth pointing out that the increment of mats electrical conductivity increases by a factor of 1×10^7 for the unfilled materials while this factor was calculated to be around 5×10^6 for the composites (Table 2). This small difference on doping efficiency is attributed to the competitive iodine vapors absorption of the nanofillers, and it is indeed a well-known fact that carbonaceous materials such as GO and rGO can absorb gasses.[49] Although the conductivity of the developed materials is calculated when the mats are completely doped (after 5 h of doping all the materials have reached their maximum level of conductivity), the nanofillers presence slightly disturbs the polymer doping process. Moreover, the absorption of I_2 molecules on rGO determines its doping and the increment of its intrinsic electrical conductivity. This additive effect that should cause the rise of the doping factor by a value higher than 1×10^7 is not visible. This fact confirms that the notable electrical conductivity achieved for P3HT/PEO/rGO is not the result of a continuous network of conductive fillers but mainly of the P3HT polymer chains and their structural improvement within the fibers.

The electrical measurement results confirmed the importance of polymers crystallinity and P3HT chains stretching in order to develop well-structured materials. They also confirmed that the control of the nanofillers orientation and the reduction of GO play crucial roles in the production with high performance materials.

CONCLUSION AND OUTLOOK

Working on this project, we have successfully developed P3HT/PEO, P3HT/PEO/GO, and P3HT/PEO/rGO composites nanofibers using the electrospinning method. Prior to the electrospinning, the GO nanosheets used as fillers were treated using a hydrothermal technique in order to produce rGO. The morphological and chemical properties of the nanofillers were studied by TEM, FT-IR, Raman spectroscopy, and TGA, while the properties of the synthesized regioregular P3HT were assessed using FT-IR, GPC, and ^{1}H-NMR.

By analyzing the developed polymer materials by SEM and TEM, we demonstrated that this experimental procedure can be used for the production of stable and reproducible GO-based and rGO-based conductive composite fibers without morphological defects. Moreover, the results of structural analysis (XRD and DSC) prove that the achieved homogeneous distribution and parallel orientation of the nanosheets along the fibers axis induce the improvement of the polymers matrix structure leading to an increase in crystallinity. The elastic modulus of single fibers and the electrical conductivity of the mats were calculated using AFM nanoindentation and a four-point method to evaluate the influence of the GO and its reduction on the nanomaterials performance. We have found that the inclusion of both GO and rGO not only similarly modified the fibers morphologies (e.g. diameters and roughness) but also their stiffness. The synergic effect of higher crystallinity and the presence of reinforcing nanomaterials led to the production of composite fibers (both P3HT/PEO/GO and P3HT/PEO/rGO) in which the value of elastic modulus is double in comparison with the mechanical properties of unfilled fibers. The results of the electrical characterization show that the control of the GO reduction is crucial for the formation of electrically conductive, high-performance nanofibers. When the as-synthesized GO is incorporated into the fibers, the measured electrical conductivity is of the same order of magnitude of the neat fibers, because the improved structure generated by the 2D-nanomaterials alignment

into the fibers is mitigated by the intrinsic dielectric properties of GO. On the other hand, the use of hydrothermally reduced GO, with the same morphological and structural features of the previous sample, led to the increment of electrical conductivity of two orders of magnitude. The rGO loading of the matrix has beneficial effects on both mechanical and electrical properties of the fibrous materials, in which the effect of the matrix properties are optimized. Furthermore, the slight reduction of GO increases its stability in the organic solvent in which the pristine ICP blends were prepared, making the nanocomposite production process easier and more stable.

Finally, this work has highlighted that the mechanical and electrical properties of electrospun conductive materials can be modulated by filling the fibers with well-dispersed and oriented GO nanosheets and by modifying the GO reduction level. Because our aim was to study the influence of GO on ICPs fibers properties, we added a second polymer to increase the starting solution spinnability and reduce the influence of morphological defects. Despite the presence of PEO within the matrix, the P3HT/PEO/rGO exhibits promising properties. This nanocomposite can be used as material for the development of flexible photovoltaic, electronic, and optoelectronic devices. With the aim to increase the successful application of this material, we will produce P3HT/rGO in the future, avoiding the use of PEO. The development of this material will be performed by dissolving PEO from the P3HT/PEO/rGO nanofibers produced in this study. An alternative approach to prepare P3HT/rGO includes the fabrication of core-shell electrospun fibers where the pure P3HT/GO composite core is confined within a shell of PEO, followed by removal of the shell. In both strategies, considering the solubility of PEO and P3HT, acetonitrile is a good candidate to be used as solvent for the selective removal of PEO.[18] Additionally, single fibers electrical conductivity will be evaluated together with the interaction of rGO with I_2 vapors and its effect on the final performance of the nanomaterial.

Overall, the development of the technique we presented and the optimization of the process parameters may have relevant implications for future applications of organic electronics.

Acknowledgements

The authors thank the University of Bologna (funds for selected research topics) for the financial support to this research. The experiments were performed using apparatus available thanks to the EC structural funds in framework of the Center for Preclinical Research and Technology (CePT), project POIG Nr. 02.02.00-17-024/08-00. We would like to acknowledge Olga Urbanek for her help with thermal analyses of the nanomaterials and Adria Costanzi for her assistance in revising the article.

REFERENCES

[1] A. G. MacDiarmid, *Angew. Chem. Int. Ed.* **2001**, *40*, 2581.
[2] N. Koch, *Chem. Phys. Chem.* **2007**, *8*, 1438.
[3] M. Lanzi, L. Paganin, F. Pierini, F. Errani, F. P. Di-Nicola, *React. Funct. Polym.* **2014**, *83*, 33.
[4] R. D. McCullough, *Adv. Mater.* **1998**, *10*, 93.
[5] F. Goldoni, D. Iarossi, A. Mucci, L. Schenetti, M. Zambianchi, *J. Mater. Chem.* **1997**, *7*, 593.
[6] J. Y. Chen, H. C. Wu, Y. C. Chiu, C. J. Lin, S. H. Tung, W. C. Chen, *Adv. Electron. Mater.* **2015**, *1*, 1400028-1400036.
[7] Y. Sharma, A. Tiwari, S. Hattori, D. Terada, A. K. Sharma, M. Ramalingam, H. Kobayashi, *Int. J. Biol. Macromol.* **2012**, *51*, 627.
[8] A. Baranowska-Korczyc, A. Reszka, K. Sobczak, B. Sikora, P. Dziawa, M. Aleszkiewicz, L. Klopotowski, W. Paszkowicz, P. Dluzewski, B. J. Kowalski, T. A. Kowalewski, M. Sawicki, D. Elbaum, K. Fronc, *J. Sol-Gel Sci. Technol.* **2012**, *61*, 494.
[9] S. J. Wu, Q. D. Tai, F. Yan, *J. Phys. Chem. C* **2010**, *114*, 6197.
[10] A. Laforgue, *J. Power Sources* **2011**, *196*, 559.
[11] A. L. Yarin, B. Pourdeyhimi, S. Ramakrishna, *Fundamentals and Applications of Micro- and Nanofibers*. Cambridge University Press, Cambridge, **2014**.
[12] L. Persano, A. Camposeo, C. Tekmen, D. Pisignano, *Macromol. Mater. Eng.* **2013**, *298*, 504.
[13] A. L. Yarin, *Polym. Adv. Technol.* **2011**, *22*, 310.
[14] D. H. Reneker, A. L. Yarin, H. Fong, S. Koombhongse, *J. Appl. Phys.* **2000**, *87*, 4531.
[15] J. Y. Chen, C. C. Kuo, C. S. Lai, W. C. Chen, H. L. Chen, *Macromolecules* **2011**, *44*, 2883.
[16] S. Lee, G. D. Moon, U. Jeong, *J. Mater. Chem.* **2009**, *19*, 748.
[17] K. H. K. Chan, T. Yamao, M. Kotaki, S. Hotta, *Synth. Met.* **2010**, *160*, 2587.
[18] A. Bianco, C. Bertarelli, S. Frisk, J. F. Rabolt, M. C. Gallazzi, G. Zerbi, *Synth. Met.* **2007**, *157*, 276.
[19] D. Kolbuk, P. Sajkiewicz, T. A. Kowalewski, *Eur. Polym. J.* **2012**, *2*, 275.
[20] M. K. Shin, S. I. Kim, S. J. Kim, S. K. Kim, H. Lee, G. M. Spinks, *Appl. Phys. Lett.* **2006**, *89*, 231929.
[21] A. Camposeo, I. Greenfeld, F. Tantussi, S. Pagliara, M. Moffa, F. Fuso, M. Allegrini, E. Zussman, D. Pisignano, *Nano Lett.* **2013**, *13*, 5056.
[22] J. Njuguna, K. Pielichowski, S. Desai, *Polym. Adv. Technol.* **2008**, *19*, 947.
[23] J. Chrzanowska, J. Hoffman, A. Małolepszy, M. Mazurkiewicz, T. A. Kowalewski, Z. Szymanski, L. Stobinski, *Phys. Status Solidi B* **2015**, *252*(8), 1860.
[24] R. H. Schmidt, I. A. Kinloch, A. N. Burgess, A. H. Windle, *Langmuir* **2007**, *23*, 5707.
[25] F. Pierini, M. Lanzi, I. G. Lesci, N. Roveri, *Fiber. Polym.* **2015**, *16*, 426.
[26] A. K. Geim, K. S. Novoselov, *Nat. Mater.* **2007**, *6*, 183.
[27] Y. Liang, D. Wu, X. Feng, K. Mullen, *Adv. Mater.* **2009**, *21*, 1679.
[28] D. R. Dreyer, S. Park, C. W. Bielawski, R. S. Ruoff, *Chem. Soc. Rev.* **2010**, *39*, 228.
[29] Y. Mao, S. Wen, Y. Chen, F. Zhang, P. Panine, T. W. Chan, L. Zhang, Y. Liang, L. Liu, *Sci. Rep.* **2013**, *3*, 2508.
[30] J. W. Suk, R. D. Piner, J. H. An, R. S. Ruoff, *ACS Nano* **2010**, *4*, 6557.
[31] C. Punckt, F. Muckel, S. Wolff, I. A. Aksay, C. A. Chavarin, G. Bacher, W. Mertin, *Appl. Phys. Lett.* **2013**, *102*, 023114.
[32] C. K. Chua, M. Pumera, *Chem. Soc. Rev.* **2014**, *43*, 291.
[33] C. Gómez-Navarro, M. Burghard, K. Kern, *Nano Lett.* **2008**, *8*, 2045.
[34] C. J. Lin, C. L. Liu, W. C. Chen, *J. Mater. Chem. C* **2015**, *3*, 4290.
[35] Z. Yang, H. Lu, *J. Appl. Polym. Sci.* **2013**, *128*, 802.
[36] E. P. S. Tan, C. T. Lim, *Compos. Sci. Technol.* **2006**, *66*, 1102.
[37] I. D. Norris, M. M. Shaker, F. K. Ko, A. G. MacDiarmid, *Synth. Met.* **2000**, *114*, 109.
[38] R. S. Loewe, S. M. Khersonky, R. D. McCullough, *Adv. Mater.* **1999**, *3*, 11.
[39] M. Lanzi, P. Costa-Bizzarri, C. Della-Casa, L. Paganin, A. Fraleoni, *Polymer* **2003**, *44*, 545.
[40] H. Chen, Z. Song, X. Zhao, X. Li, H. Lin, *RSC Adv.* **2013**, *3*, 2971.
[41] D. Konios, M. M. Stylianakis, E. Stratakis, E. Kymakis, *J. Colloid Interface Sci.* **2014**, *430*, 108.
[42] H. Becerril, J. Mao, Z. Liu, M. Stoltenberg, Z. Bao, Y. Chen, *ACS Nano* **2008**, *2*, 463.
[43] A. Laforgue, L. Robitaille, *Synth. Met.* **2008**, *158*, 577.
[44] S. Panzavolta, B. Bracci, C. Gualandi, M. L. Focarete, E. Treossi, K. Kouroupis-Agalou, K. Rubini, F. Bosia, L. Brely, N. M. Pugno, V. Palermo, A. Bigi, *Carbon* **2014**, *78*, 566.
[45] C. Gerbaldi, J. R. Nair, M. A. Kulandainathan, R. S. Kumar, C. Ferrara, P. Mustarelli, A. M. Stephan, *J. Mater. Chem. A* **2014**, *2*, 9948.
[46] J. C. Lin, W. Y. Lee, H. C. Wu, C. C. Chou, Y. C. Chiu, Y. S. Sun, W. C. J. Chen, *Mater. Chem.* **2012**, *22*, 14682.
[47] L. Sun, J. T. Yang, G. Y. Lin, M. Q. Zhong, *Mater. Lett.* **2007**, *61*, 3963.
[48] B. O'Connor, E. P. Chan, C. Chan, B. R. Conrad, L. J. Richter, R. J. Kline, M. Heeney, I. McCulloch, C. L. Soles, D. M. DeLongchamp, *ACS Nano* **2010**, *4*, 7538.
[49] H. Kim, O. Renault, A. Tyurnina, J. P. Simonato, D. Rouchon, D. Mariolle, N. Chevalier, J. Dijon, *Appl. Phys. Lett.* **2014**, *105*, 011605.

